Journal of Alloys and Compounds 854 (2021) 157113

Contents lists available at ScienceDirect

Journal of Alloys and Compounds

journal homepage: http://www.elsevier.com/locate/jalcom

Correlating the gradient nitrogen doping and electromagnetic wave absorption of graphene at gigahertz

Mingqiang Ning, Boya Kuang, Lin Wang, Jingbo Li*, Haibo Jin**

Beijing Key Laboratory of Construction Tailorable Advanced Functional Materials and Green Applications, School of Materials Science and Engineering, Beijing Institute of Technology, Beijing, 100081, PR China

ARTICLE INFO

Article history:
Received 20 July 2020
Received in revised form
28 August 2020
Accepted 8 September 2020
Available online 9 September 2020

Keywords:
Nitrogen doping
Attenuation factor
Impedance matching
CST simulation
Microwave absorption

ABSTRACT

Nitrogen doping has been proved an effective strategy to improve the microwave absorption performance of graphene. However, the detailed investigations correlating the role of nitrogen dopants with dielectric properties and microwave absorption of graphene has not been available. In this work, the gradient nitrogen doped graphene (NG with 0 wt%, 3.7 wt% and 6.86 wt% N content) were prepared *via* a facile hydrothermal strategy. The effect of nitrogen dopant on microstructure, morphology, chemical composition, complex permittivity, attenuation factor, impedance matching degree and microwave absorption of graphene were systematically investigated. The electromagnetic characterization and CST simulation results reveal that the moderate N-doped graphene (NG-100) endows the optimal microwave absorbing performance, which was attributed to the moderately introduced dipole polarizations, as well as the better balance between attenuation factor and impedance matching degree. The maximum reflection loss (RL_{max}) of NG-100 is ~ -55 dB under 3.2 mm, which is five times higher than that of non-doped graphene. Meanwhile, the effective attenuation bandwidth (EAB: < -10 dB) of NG-100 is up to ~6.82 GHz under 2.6 mm. More importantly, by correlating gradient N-doped graphene with attenuation factor and impedance characteristics, this work provide an approach to the design and construction of graphene-based composites as efficient microwave absorber for realizing practical applications.

1. Introduction

Nowadays, with the rapidly development of information technology in both civil and military fields, lightweight and high-efficiency electromagnetic wave (EMW) absorption over wide frequency range are desired properties for EMW attenuation absorbers [1–6]. Among many kinds of EMW absorbers, carbon materials, including carbon nanosheets (CNSs) [7], carbon nanotubes (CNTs) [8,9], carbon nanocoils (CNCs) [10] *etc.* Have been long considered as candidates for high efficiency EMW absorption application due to their lightweight and high EMW absorbing ability. Graphene, as the dramatic two dimensional (2D) material, has also attracted extensive interests in EMW absorbing fields in recent years. For example, Chen et al. reported the broadband and tunable high EMW absorbing performance of three dimensional (3D) free-standing graphene foam (GF), which could be ascribed to the unique 3D conductive network [5]. They also prepared the ultralight multi-walled carbon nanotube/graphene foams (MWCNT/CGFs) and attributed the excellent EMW absorbing performance to the 3D high loss multilevel network and good balance between impedance matching and attenuation ability [4]. However, the sole graphene absorber still suffer from impedance mismatching issue due to its intrinsic Fermi level structure and limited EMW attenuation mechanisms [11,12]. Therefore, the researchers are always looking for new strategies to boost the EMW attenuation ability of graphene-based composites.

According to previous studies [12–15], constructing nanostructures toward graphene (*eg*: decorating graphene with magnetic nanoparticles) are beneficial to optimize the impedance matching and broaden the effective attenuation bandwidth (EAB, RL < -10 dB). Mahmood et al. [14]. reported the Fe_3O_4/graphene capsules (GCs) composites with a RL_{max} value of −32 dB at 8.76 GHz under 3.5 mm. Cao et al. [15] prepared the 3D flower-like Co_3O_4/rGO and the RL_{max} reached ~ -61 dB under 3 mm. He et al. [13]. found that $NiFe_2O_4$ nanoparticles decorated rGO ($NiFe_2O_4$/rGO) exhibited good EMW absorbing performance: the RL_{max}

* Corresponding author.
** Corresponding author.
E-mail addresses: lijb@bit.edu.cn (J. Li), hbjin@bit.edu.cn (H. Jin).

https://doi.org/10.1016/j.jallcom.2020.157113
0925-8388/

exceeded −42 dB with an EAB of 5.3 GHz under 5 mm. However, for achieving a better EMW absorbing performance, the percentage of those graphene-based composites in matrix (such as Wax, PVdF or SiO_2) was usually high (30 wt%, 50 wt% or even 70 wt%), which does not meet the "light" requirement of EMW absorbers [13–15]. Additionally, magnetic particles generally follow Snoek's limit (*i.e.* the magnetic loss mechanism does not work at a frequency higher than its resonant frequency [13,16]. As a result, the nanostructure constructing strategy toward graphene has its limitations at high frequencies.

Element doping is another effective strategy to tune the physicochemical properties of graphene, thus achieving the tailored performance in the area of EMW attenuation [17–19]. According to the reports [20–23], the doping strategy not only helps boost the conductivity and facilitate the conductive loss, but also introduces a numbers of heterogeneous atom defects during the doping process, thus alleviating the attenuation ability of absorbers. Nitrogen (N), as the neighbor of carbon element in periodic table, is the most widely studied dopant for carbon materials [21,23–25]. In EMW absorption areas, various N-doped carbon hybrids have been studied in past decade in. For example, Kamal K. Kar et al. reported the microwave absorption performance of N-doped graphene nanosheet-epoxy nanocomposite, where the electric, dielcetric, interficial polarization was thought as the main EMW attenuation mechanisms [26]. Liu and co-workers also studied the excellent electromagnetic wave absorption properties of three-dimensional lightweight nitrogen-doped graphene aerogel by hydrothermal method. According to their results, the NG absorber with 3.6 wt% loading displayed the most excellent microwave absorption properties [23]. Besides the pure N-doped graphene absorber, the NG coupled with other dielectric/magnetic kind componenets were also widely adopted in this area. Chen and co-workers [27,28] prepared the 3D NiFe/N-CNT and FeNi@N-doped graphene, which display excellent EMW attenuation ability (−40.3 dB and −39.39 dB) and EAB (4.5 GHz and 4.7 GHz). Kamal K. Kar [29] et al. reported EMW attenuation performance of N-doped carbon materials derived from chicken feather fibers with a RL_{max} of −20.1 dB and a EAB of 2.9 GHz under 2.0 mm. Moreover, the N-doped graphene aerogel [23], Co/CNTs/carbon sponge [30] and M@N-CNTs (M = Fe, Co and Ni) [8] were also studied as efficient EMW absorbers. In those composites, the optimized consumption of EMW were usually attributed to the defect-dipole polarizations introduced by nitrogen doping. As a contrast, compared to those carbon or graphene-based absorbers, there are rare literatures have systematically studied the detailed N doping effect toward the pure graphene (such as impedance degree and the proper threshold content *etc.*) to our best knowledge. In other words, there are still rare reports to correlating the nitrogen doping content with the exact electromagnetic behaviors of pure graphene. Therefore, it is highly desired but challenging to study the underlying beneficial effects of heteroatom doping considering the fundamental research toward the basic EMW starting material (*i.e.* graphene). Flgurthermore, the exact N-doping research toward graphene can be applicable to a wide range of graphene-based EMW absorbers and support for the fabrication of novel EMW composites.

Herein, to correlate the nitrogen doping effects with EMW absorbing of graphene at gigahertz, the gradient N-doped graphene (NG) was rationally prepared by adjusting the mass ratio of GO and urea in the hydrothermal reaction. When applied as EMW absorber, the moderately nitrogen-doped NG (~3.7 wt% N content) exhibits the optimal EMW absorbing with a RL_{max} of ~ -55 dB under 3.2 mm. The experimental and CST simulation results reveal that the optimized EMW absorbing performance of NG was ascribed to the better balance between the attenuation factor (α) and impedance matching degree (Δ). Based on those results, the relationship between N-doping content and dilectric and EMW absorbing performance were built.

2. Experimental section

2.1. Preparation of gradient N-doped graphene

The graphene oxide (GO) was prepared from graphite powder by a modified Hummers' method and the NGs were prepared *via* a mild hydrothermal process [3,13,15,24]. The detailed synthesis process is depicted as shown in Fig. 1. In a typical procedure, 20 mg GO was combined with 10 mL deionized water and further sonicated for 1 h to yield a dark brown suspension. Then, 2 g urea was added to the above solution and the whole solution were sonicated for 1 h. To obtain the gradient N-doped graphene, the mass ratio of urea and GO is set to 100:1 and 240:1 (denoted as NG-X and X is 100 and 240, respectively). Next, the mixture was transferred to a Teflon-lined autoclave and heated to 110 °C for 10 h. Finally, the products were immersed in deionized water for 12 h and finally obtained by freeze drying treatment (Fig. 1 step I). The rGO absorber was prepared by the similar procedure as that of NG except without adding urea.

2.2. Preparation of NG-X/wax and electromagnetic measurement

(i) Specific quantities of paraffin wax (97.5, 95 and 92.5 wt% vs. absorbers) were completely dissolved in appropriate amount of ether under stirring; (ii) Specific quantities of absorbers (2.5 wt%, 5 wt% and 7.5 wt% vs.wax) were added into the solution and stirred vigorously; (iii) The whole solution were subjected to the ultrasonic treatment under stirring; (iv) After the ether were evaporated completely, the solid samples were pressed into the required shape for the measurement (outer radius: 7.00 mm; inner radius: 3.04 mm) for dielectric measurement by coaxial method over 2–18 GHz on Anritsu 37269 D vector network (Fig. 1 step II).

2.3. CST simulation

The power flow, electric field and power loss density were simulated using the finite integration technique on Computer Simulation Technology (CST) Microware Studio software. Ten layers lamina with a thickness of 0.32 mm were constructed as the unit absorber cell. The unit cell was set with periodic boundary conditions in X/Y plane and the EMW was generated along -Z direction (Fig. 1 step III and Fig. S8). During simulation processes, the experimental measured electromagnetic parameters of three asborbers were used as complex permittivity and permeability of rGO and NG-X absorbers.

2.4. Characterization

Powder X-ray diffraction (XRD) patterns were collected on a Bruker-AXS diffractometer (Cu-$K\alpha$). Scanning electron microscopy (SEM) and transmission electron microscope (TEM) images were obtained using Hitachi S-480 and FEI Tecnai G2 F20S-TWIN. Raman spectra measurements were performed on a Lab RAM Aramis. X-ray photoelectron spectroscopy (XPS) was carried out on a PHI Quantera. Fourier transform infrared spectroscopy (FT-IR) was carried out on a Thermo Fisher Scientific™ Nicolet™ iS™ 50 and the scanning range of the wavenumber was 400–4000 cm^{-1}. Electrical conductivity of NG was performed by four-point probe (Keithley 4200-SCS) measurements.

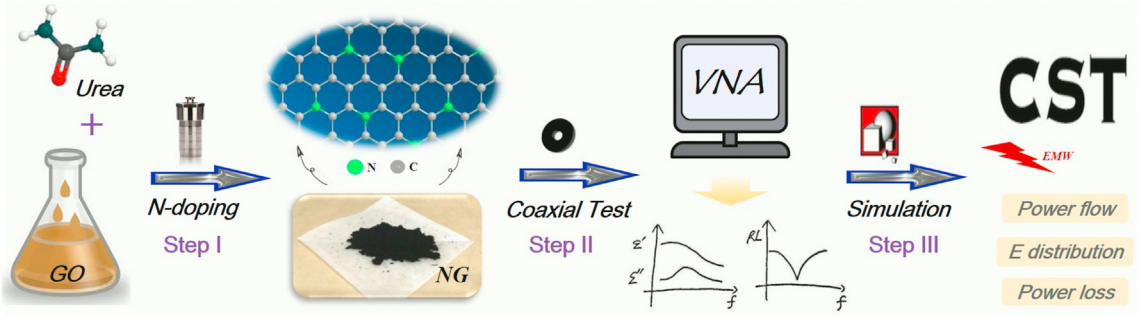

Fig. 1. Schematic illustration of the fabrication, measurement and CST simulation processes toward NG-X.

3. Results and discussions

3.1. Morphologies and nanostructures

SEM images of GO, rGO and NG-X are presented in Fig. S1 (a-d). As can be seen, GO and rGO samples exhibit thin and crumpled sheets with random aggregations (Fig. S1 a-b). After nitrogen doping treatment, the NG-X are composed of relatively ultrathin 2D nanosheets with edges rolled up due to surface tension [24,31,32]. To further investigate the crumpled and corrugated structures of rGO and NG-X, the TEM and elemental mapping characterization were carried out.

Fig. 2(a–c) show the TEM images of rGO, NG-100 and NG-240. The typical rippled and entangled 2D graphene sheets were observed to be situated on copper grid. High resolution transmission electron microscopy (HRTEM) images of rGO, NG-100 and NG-240 also exhibited the typical wrinkled morphologies with a mixture of single and few-layer graphene nanosheets as shown in Fig. S2. The selected area electron diffraction (SAED) of rGO (Fig. 2) indicates the graphene are of graphitic laminar structure of stacks [33–35]. The HAADF elemental mapping images show that the C, O, N elements were homogenously distributed throughout the NG-X absorbers (Fig. 2 b and c), indicating the successful nitrogen doping in NG-X. Specially, compared to the pale green nitrogen mapping of NG-100, the deep yellow nitrogen mapping implies the increased N-doping content of NG-240. Fig. 2 (d) are the compared histograms of C, N and O elements in three absorbers (detailed dates were provided in Table S1). As clearly presented, the weight and atomic ratio of N element in three samples presente the linear upward trend (0 wt%, 3.7 wt% and 6.86 wt%, respectively), indicating the gradient nitrogen doping toward graphene. In addition, the weight and atomic ratio of C and O elements exhibite minor fluctuation trend according to that of N element.

Fig. 3 (a) shows the structure evolution of GO to NG-X characterized by XRD. The GO displays a strong characteristic peak at 2θ~10.2°, due to the formation of functional groups in the basal surface [31,36]. Upon reducing by hydrothermal and nitrogen doping reaction, the peak located at ~10.2° disappears, and a broaden peak around ~23° is alternatively observed, which is the typical rGO pattern [13,36]. It is noteworthy that the broaden peak around 2θ~23° shifts to higher angle, indicating the decreased interlayer distance because of the partial removal of functional groups as the amount of urea increases [25,31].

Fig. 3 (b) shows the Raman spectra of rGO and NG-X absorbers. Two characteristic peaks around ~1347 cm^{-1} and ~1581 cm^{-1} correspond to the so-called *D* band and *G* band [37]. In general, *D* band is a typical sign of the presence of defective graphitic carbon and *G* band is the characteristic feature of graphitic carbon layers corresponding to the vibration of sp^2-bonded carbon atoms in 2D hexagonal lattices [37,38]. The intensity ratio of *D* band and *G* band (I_D/I_G) is usually used as an indicator of the lattice-defect density in carbon materials. The more lattice-defects exist, the higher intensity of I_D/I_G value [39]. In this work, the I_D/I_G ratio of GO, rGO and NG-X are calculated to be ~0.97, ~1.0, ~1.08 and ~1.12, respectively, suggesting the increased point defects (such as C vacancies and doped N atoms) during the reduction and nitrogen doping process.

Fig. 3 (c) presents the FT-IR spectra of rGO and NG-X. The relative strong peaks of GO and rGO located at ~3420 cm^{-1}, ~1728 cm^{-1}, ~1630 cm^{-1}, ~1218 cm^{-1} and ~1055 cm^{-1} are ascribed to the stretching vibration of water molecules (O–H), carbonyl (C=O), aromatic skeleton carbon ring (C=C), hydroxyl (C–OH) and alkoxy (C–O), respectively [40]. After nitrogen doping treatment, these absorption peaks nearly disappear, suggesting the removal of most oxygen functional groups. However, two new absorption peaks of NG-X located at ~1193 cm^{-1} and ~1550 cm^{-1} are observed, which correspond to the stretching vibration of C–N and C=N [26], implying the successful nitrogen doping in NG-X absorbers.

XPS measurements were carried out to examine the chemical states of elements in GO and NG-X absorbers. Fig. 3 (d) displays the XPS full spectra of GO, rGO, NG-100 and NG-240, which clearly indicates the existence of nitrogen element in NG samples. The mass percentages of N atoms in NG-100 and NG-100 are measured to be ~2.9 wt% and ~8.9 wt% as revealed by XPS characterization (detailed dates were provided in Table S2). It is clear that the content of doped-nitrogen in NG-X samples also presents an upward trend with the increasing amount of urea. It is worth noting that the N-doped content revealed by XPS measurement are consistent with that of EDS mapping results (Table S1) when taking the measurement error into account.

To further figure out the configuration of C, O and N elements, the C 1s, O 1s and N 1s high-resolution XPS peaks of NG-X are collected. Fig. S3 shows the detailed deconvoluted peaks of C 1s and O 1s. As for N 1s peak as displayed in Fig. 3 (e and f), it can be well deconvoluted into graphitic N (~401.8 eV) and oxidized N (~402.9 eV), respectively [21]. The graphitic N related defective structures are schematically illustrated in Fig. 3 (g). According to previous reports [8,20,36], those defects could act as dipoles under EMW field to enhance the dielectric loss of absorbers. It is well known that the nitrogen doping also affects the graphene's electric properties by donating electrons and thereby shifting its Fermi level (ΔEF) as Fig. 3 (i) shown [41,42]. As a result, the electrical conductivity (σ) of NG-X/wax rationally delivers an increasing trend, *i.e.* from ~4×10^{-2} S/m to ~8×10^{-1} S/m and ~10.0 S/m as the increasing of nitrogen doping content (Fig. 3 h). According to previous reports [3–5,7,15,20], the suitable conductivity of absorbers could give rise to a benefit to the attenuation of EMW.

3.2. Dielectric properties

The permeability (μ_r) and permittivities (ε_r) of absorbers with 2.5 wt%, 5 wt% and 7.5 wt% mass loadings over 2–18 GHz were measured using coaxial method as described in Experimental

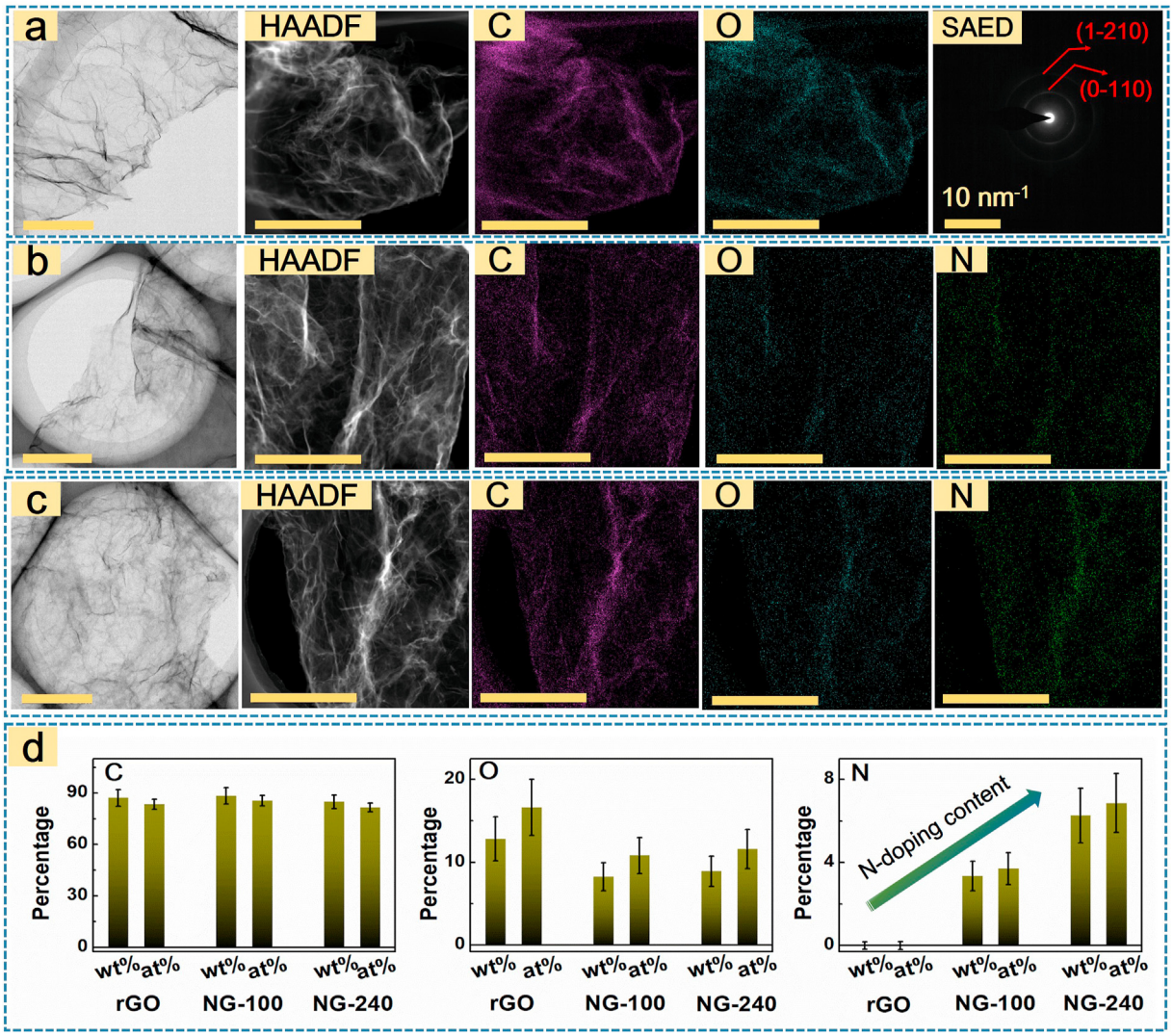

Fig. 2. TEM images of (a) rGO, (b) NG-100 and (c) NG-240; the following images in (a, b and c) are the HAADF-STEM images and the corresponding mappings of C, N and O (the bars are 1 μm); (a-4) is the SAED images of rGO; (d) is the wt% and at% histogram images of C,N and O elements in three absorbers.

section 2.2. The complex permeability values (μ' and μ'') were measured ~1.0 and ~0, thereby suggesting a negligible magnetic loss in non-magnetic graphene absorbers (Fig.S6). As for the dielectric spectra, both the ε' and ε'' of rGO and NG-X present the upward trend as the increasing of mass loadings over the explored frequency (Fig. 4 a-f). According to the effective medium theory [2–4], the polarizable charges in absorber are on the increase with the increasing of mass loadings, leading to the increase of ε'. As for the ε'', ε'' is governed by the polarization part (ε''_p) and electrical conductivity part (ε''_c) according to the well-known Debye theory (Eqn. (1)) as follows [7,28,43,44],

$$\varepsilon'' = \frac{\varepsilon_s - \varepsilon_\infty}{1+\omega^2\tau^2}\omega\tau + \frac{\sigma}{\omega\varepsilon_0} = \varepsilon''_p + \varepsilon''_c \quad (1)$$

where τ is the polarization relaxation time, ω the angular frequency, ε_s the static permittivity and ε_∞ the relative dielectric permittivity at the high frequency limit. Considering the existing of functional groups (such as C=O, C–OH and C–O) and the increase of lattice defects with the N content as evidenced by EDS (Fig. 2 d), Raman (Fig. 3 b) and XPS results (Fig. 3 e-f), the polarization loss should also enhance because the lattice defects could act as electric dipole under alternative EMW field [45,46]. Meanwhile, with the increasing of nitrogen content in absorbers, the conduction loss of NG also presents an upward trend as that of σ (Fig. 3 h), which is consistent with the results as reported in previous work [8,32]. Therefore, it is also rational to observe the increase of ε'' with the increasing mass loading and nitrogen doping content.

To evaluate the attenuation ability of absorbers, the dielectric loss tangents ($tan\ \delta_E = \varepsilon''/\varepsilon'$) were deduced and plotted as shown in Fig. S4. One can find that the order of dielectric loss capability presents the upward trend (NG-240 > NG-100 > rGO) as that of ε' and ε'' under different mass loadings, verifying the enhanced dielectric loss ability as the increasing doping toward graphene. Typical Cole-Cole plots were also curved to analysize the EMW attenuation mechanism of NG absorbers (Fig. S5). The semicircles and linear tail presented by three absorbers confirms the extience of Debye relaxation and conductive loss [17,47]. Compared to small numbers of defects in rGO (dangling bond, C points defects *etc.*), the N-related defects (mainly the graphitic N defects as evidenced in Fig. 3(e and f) were introduced in large numbers. Consequently, the whole polarity of system (C and N species) will be enhanced , which was beneficial to increase the charge density distribution in absorbers according to the theoretical calculations [44]. The

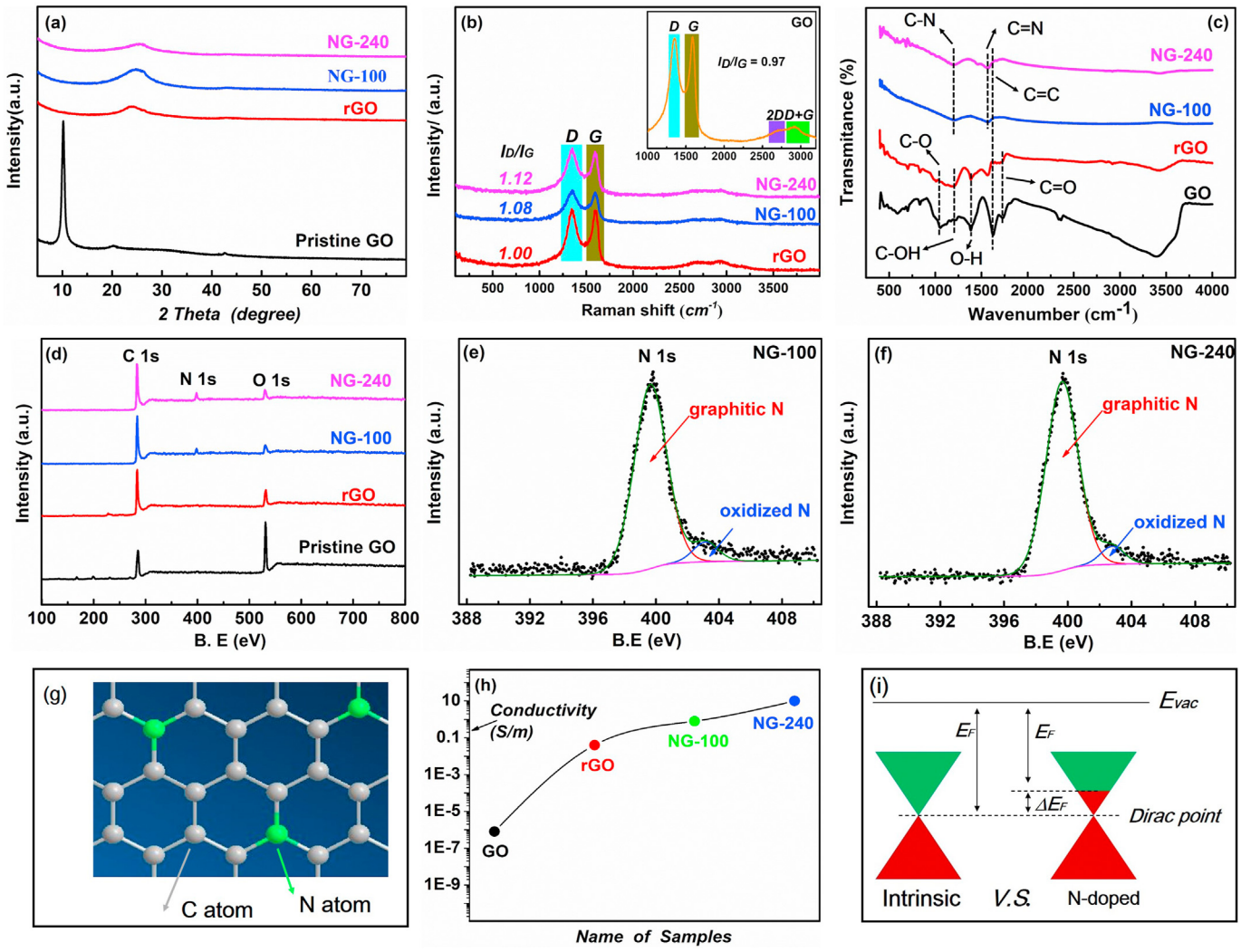

Fig. 3. (a) XRD patterns, (b) Raman, (c) FT-IR and (d) full XPS spectra of GO, rGO and NG-X; the deconvoluted N1s spectra of (e) NG-100 and (f) NG-240; (g) the illustration of N bonding in graphene; (h) the σ evolution curve of GO/wax, rGO/wax and NG-X/wax; (i) the energy band diagrams of pristine graphene and NG-X.

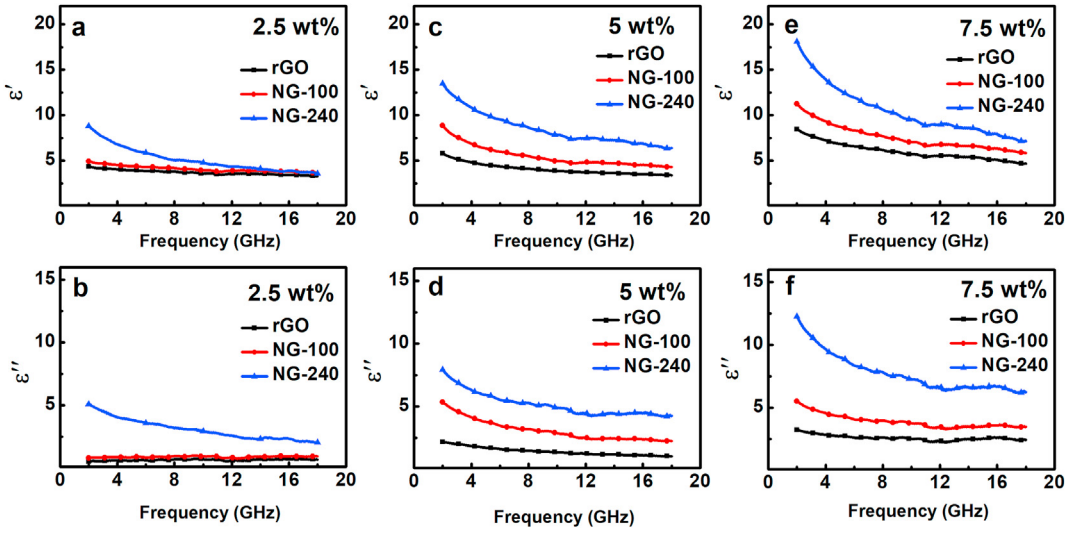

Fig. 4. ε_r-f curves of (a, b) rGO, (c, d) NG-100 and (e, f) NG-240 absorbers with 2.5 wt%, 5 wt% and 7.5 wt% mass loadings.

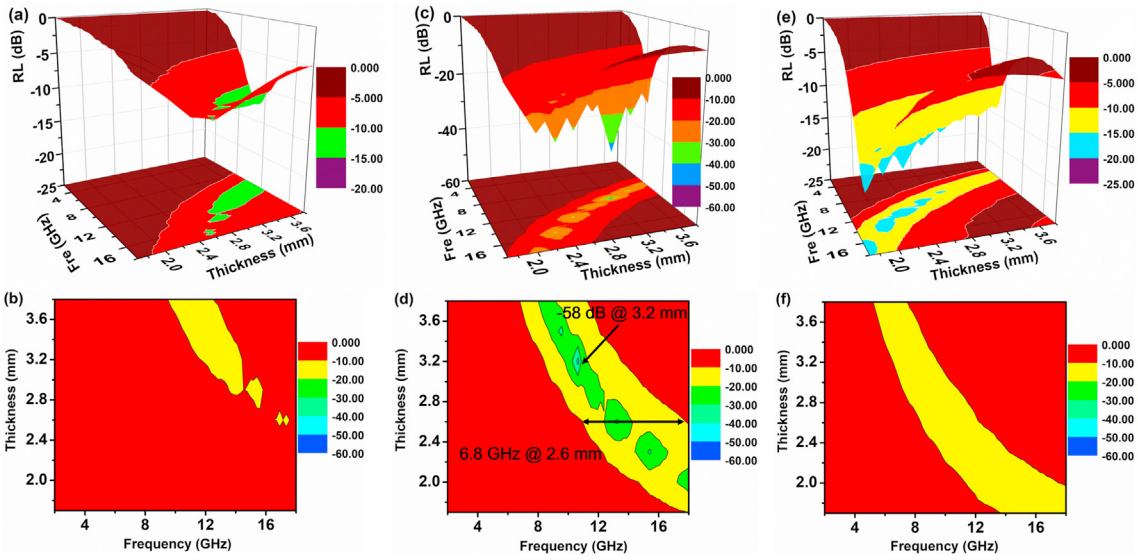

Fig. 5. 3D *RLs* and 2D projection plots of (a, b) rGO, (c, d) NG-100 and (e, f) NG-240 absorbers with 5 wt% mass loading under 1.7–3.8 mm.

semicircles (marked by colored lump) of NG-X were obvioulsy stronger that of rGO absorber (Fig. S5), further indicating the boosted dielectric relaxation in those N-doped absorbers [8,47].

3.3. Microwave absorption performance

The *RLs-f* curves of three absorbers are calculated according to the transmission line theory (Eqns. (2) and (3)) as follows [2,7],

$$Z_{in} = Z_0\sqrt{\mu_r/\varepsilon_r}\tanh\left[j\cdot\frac{2\pi f}{c}\cdot d\cdot\sqrt{\mu_r\varepsilon_r}\right] \quad (2)$$

$$RL = 20\cdot\lg\left|\frac{Z_{in}-Z_0}{Z_{in}+Z_0}\right| \quad (3)$$

where Z_{in} the input impedance of the absorber, Z_o the characteristic impedance of free space, c the light velocity, f the electromagnetic wave frequency and d the thickness of absorbers. Fig. 5 (a, c and e) display the 3D *RLs-f* plots of rGO, NG-100 and NG-240 with 5 wt% loading by manipulating the thickness from 1.7 to 3.8 mm. The corresponding 2D *RLs-f* plots display that rGO and NG-X absorbers can consume the incident EMW as presented by the yellow area of less than −10.0 dB (90% adsorption). By comparison, it is easy to observe that the N-doped graphene absorbers endow the boosted EMW absorbing performance with respect to pristine rGO absorber. Especially, the moderate N-doped absorber (NG-100) gives the optimum RL performance among three absorbers with a RL_{max} of ~ -55 dB under 3.2 mm and a EAB of 6.8 GHz under 2.6 mm (Fig. 5 b, d and f). Fig. S7 show the detailed *RLs-f* curves of rGO and NG-X with 2.5 wt%, 5 wt% and 7.5 wt% loadings under 1.7–3.8 mm. The *RLs* peaks of rGO, NG-100 and NG-240 shift toward low frequency with increasing of thickness, confirming the quarter wavelength attenuation principle [2,8,30]. For rGO absorber, the EMW absorbing performance increases as the mass loading increases from 2.5 wt% to 7.5 wt%. For rGO with 7.5 wt% loading, the RL_{max} is ~ -23 dB and EAB up to 5.75 GHz under 2.3 mm. The EMW absorbing performance of NG-100 and NG-240 presents the similar trend with that of rGO under 2.5 wt% and 5 wt%, however, becomes worse as the mass loading is 7.5 wt%. For NG-240 with 2.5 wt% loading, the RL_{max} is ~ -24.9 dB under 2.6 mm and EAB is ~7.36 GHz under 3.2 mm. In addition, by comparing three samples under the same thickness and mass loading, the *RLs* peaks shift toward lower frequencies with the increasing of N-doped content, which is consistent with the increasing trend of dielectric constants as N-

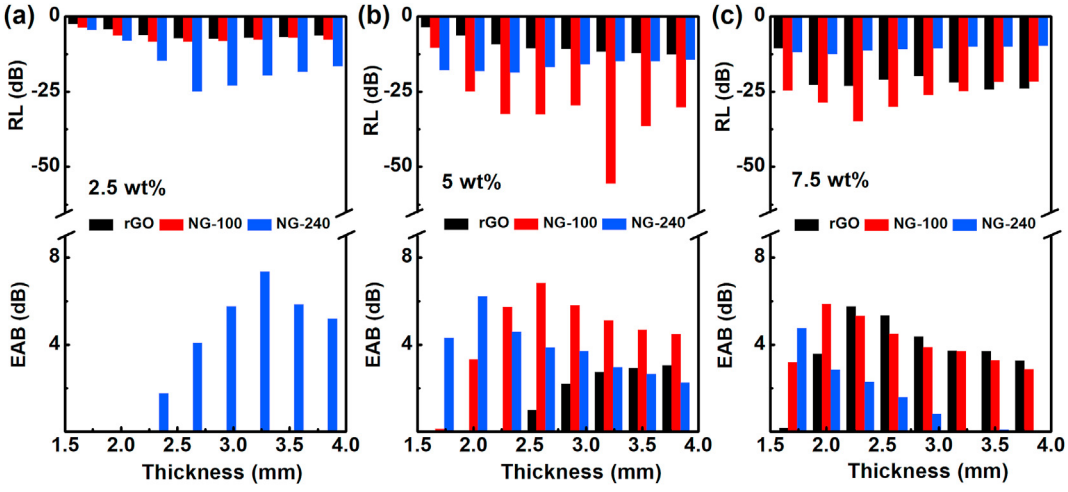

Fig. 6. Comparison of *RLs* and *EAB* (<-10 dB) values of rGO, NG-100 and NG-240 with (a) 2.5 wt%, (b) 5 wt% and (c) 7.5 wt% loading under 1.7–3.8 mm.

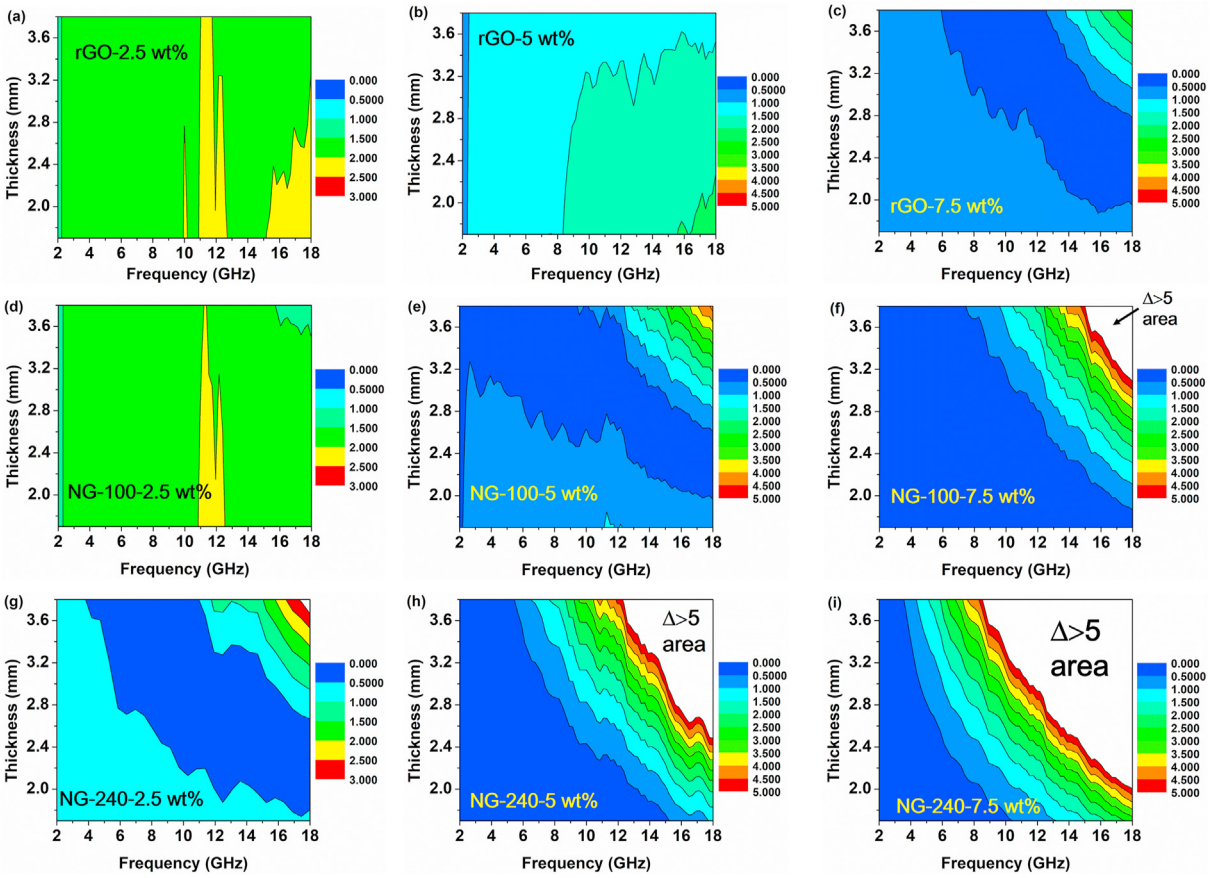

Fig. 7. 2D *Δ-f* maps of (a, b and c) rGO, (d, e and f) NG-100 and (g, h and i) NG-240 with (a, d and g) 2.5 wt%, (b, e and h) 5 wt% and (c, f and i) 7.5 wt% mass loadings under 1.7–3.8 mm.

doped content increases (Fig. 4).

Fig. 6(a–c) depicts the *RLs-thickness* and *EAB-thickness* comparison histograms of rGO and NG-X absorbers with different loadings under 1.7–3.8 mm. It shows that the moderate doped graphene (NG-100) presents the optimized EMW absorbing performance, while the heavy doped graphene (NG-240) displays the advantage in less mass loading (2.5 wt%) in terms of *EAB* and RL_{max} values.

3.4. Attenuation and impedance characteristics

In general, the good balance between attenuation factor (α) and impedance matching degree (Δ) is the necessary prerequisite for obtaining satisfied EMW absorbing performance. A higher attenuation factor means that the EMW absorbers endow higher EMW dissipate ability, while Δ closed to 0 indicating the optimal matching characteristic [29,46,48].

To understand the underlying attenuation mechanism of NG absorbers, the α and Δ values of rGO, NG-100 and NG-240 absorbers are calculated by Eqns (4) and (5) as follows [30,48–51],

$$a = \frac{\sqrt{2}\pi f}{c}\sqrt{(\mu''\varepsilon'' - \mu'\varepsilon') + \sqrt{(\mu''\varepsilon'' - \mu'\varepsilon')^2 + (\mu'\varepsilon'' + \mu''\varepsilon')^2}} \quad (4)$$

$$\Delta = \left|\sinh^2(Kfd) - M\right| \quad (5)$$

$$M = \frac{4\varepsilon'\cos(\delta_E)\mu'\cos(\delta_M)}{[\mu'\cos(\delta_E) - \varepsilon'\cos(\delta_M)]^2 + \left(\tan\frac{\delta_M - \delta_E}{2}\right)^2[\mu'\cos(\delta_E) + \varepsilon'\cos(\delta_M)]^2}$$

$$K = \frac{4\pi}{c}\sqrt{\varepsilon'\mu'}\,\frac{\sin\left(\frac{\delta_M + \delta_E}{2}\right)}{\cos(\delta_E)\cdot\cos(\delta_M)}$$

$$\delta_E = \arctan\left(\frac{\varepsilon''}{\varepsilon'}\right)$$

$$\delta_M = \arctan\left(\frac{\mu''}{\mu'}\right)$$

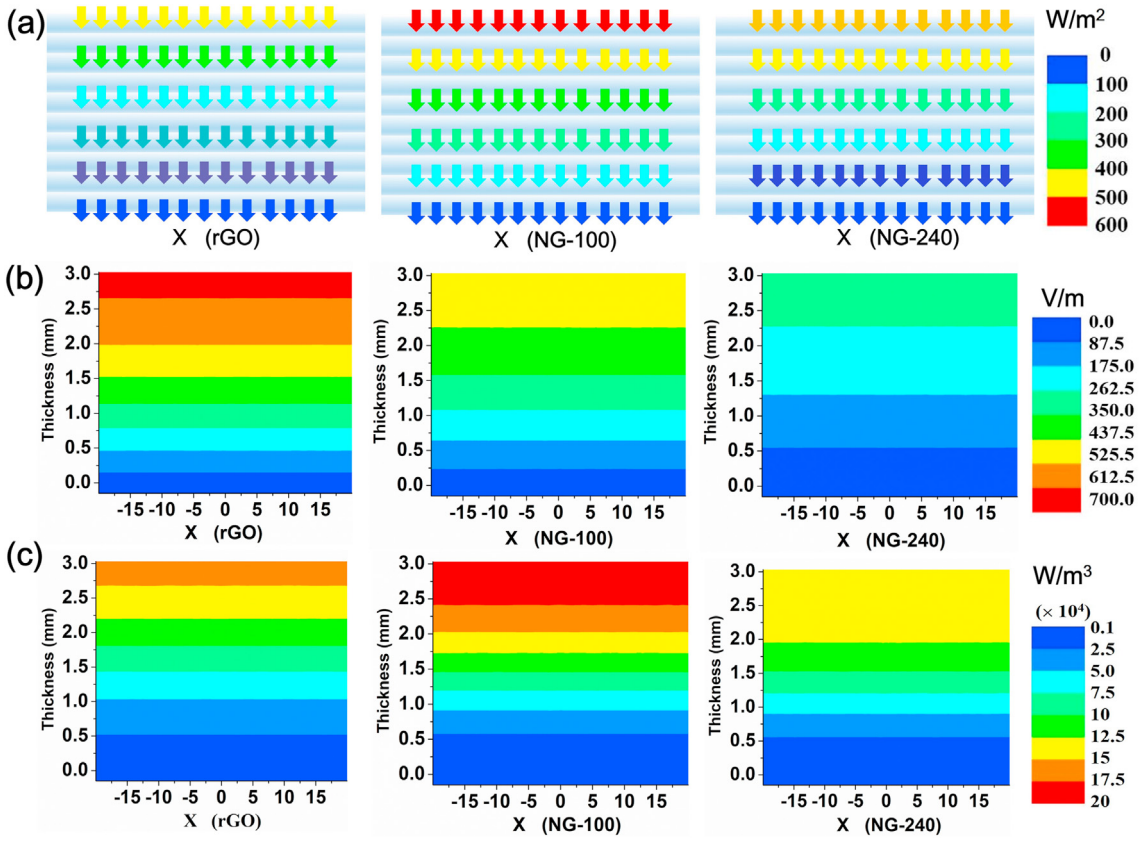

Fig. 8. (a) power flow, (b) electric field and (c) power loss density distribution diagrams of rGO, NG-100 and NG-240 with 5 wt% loading under 3.2 mm at 10 GHz.

Fig.S 9 (a-c) show the α-f curves of rGO, NG-100 and NG-240 absorbers. Apparently, the α value of absorbers show an linear upward trend wth a range of 120−1100, indicating the enhanced EMW attenuation ability as the gradient increased of nitrogen content, which provided the premise for using as high performance EMW absorbers.

Fig. 7(a−i) display the 2D Δ-f maps of rGO, NG-100 and NG-240 absorbers with 2.5, 5 and 7.5 wt% mass loadings under 1.7−3.8 mm. By comprehensive comparison the satisfied matching regions (as blue as possible) under different mass loadings, it is found the NG-100 displays the optimal Δ values, showing the beneficial effects of moderate N-doping. However, it is worth noting that the rGO absorber still possess the impedance matching advantage at high frequencies (Fig. 7 c). As the increasing of N-doping content, the NG-240 gives the optimal Δ values under 2.5 wt% (Fig. 7 g), further implying the advantages of less mass loading under heavy doping. According to previous studies [17,49] and above nanostructure analysis, the impedance matching evoluation of NG-X absorebers should be attributed to the introduced defect-dipole polarization and conductive loss by nitrogen doping. In details, moderate N-doped NG-100 endows the moderate σ values and defect polarization, which ameliorates the entering of incident EMW inside of absorbers. As for NG-240, the increased N-doping content in graphene can still optimized the matching characteristic under 2.5 wt %. However, the increasing of mass loading (5 and 7.5 wt%) lead to the deterioration of Δ values as shown in Fig. 7(h and i). This should be attributed to the dramatical decreased skin depth ($\delta=(\pi f\mu\sigma)^{-1/2}$) when the σ of NG-240 exceeds the threshold values [3,12,20]. Considering the better combination between α and Δ, NG-100-5 wt %, NG-100-7.5 wt% and NG-240-2.5 wt% absorbers should possess the relative satisfied EMW absorbing performance, which is also cnsistent with that of RL-f curves as shown in Fig. S7. However, it should note that the rGO still possesses the advantage of with high mass loading (7.5 wt% as shown in Fig. 6 c).

3.5. CST simulations

To further intuitively confirm and exhibit the beneficial effects of good balance between "α" and "Δ", the CST simulated power flow (W/m^2), electric field (V/m) and powder loss density (W/m^3) distribution diagrams of rGO and NG-X absorbers are carried out. First, the CST study model were verified by comparing the S parameters (S11: dB) with the calculated RLs. As shown in Fig. S 10 (a-c), the CST simulated S11 of rGO and NG-X (5 wt% under 3.2 mm) were well comsistent with the calculated RL curves, implying the proper construction of study model. On the basic of this model, the power flow density, electric field and power loss density were simulated. The power flow density (W/m^2) were calculated by Eqns (6) and (7) as follows,

$$\overrightarrow{S_{av}} = \frac{1}{T}\int_0^T \vec{S}\,dt = \frac{1}{2}\mathrm{Re}[\vec{E}\times\vec{H}] \tag{6}$$

$$\vec{S} = \vec{E}\times\vec{H} \tag{7}$$

According to the arrows marked with different color fill as shown in Fig. 8 (a), one can find that the power flow entering absorbers presents the trend in the order of NG-100 > NG-240 > rGO, further verifying the impedance characteristics of three absorbers as demonstrated in Fig. 7 (b, e and h). Fig. 8 (b and c) show the electric field (V/m) and power loss density (W/m^3) of three

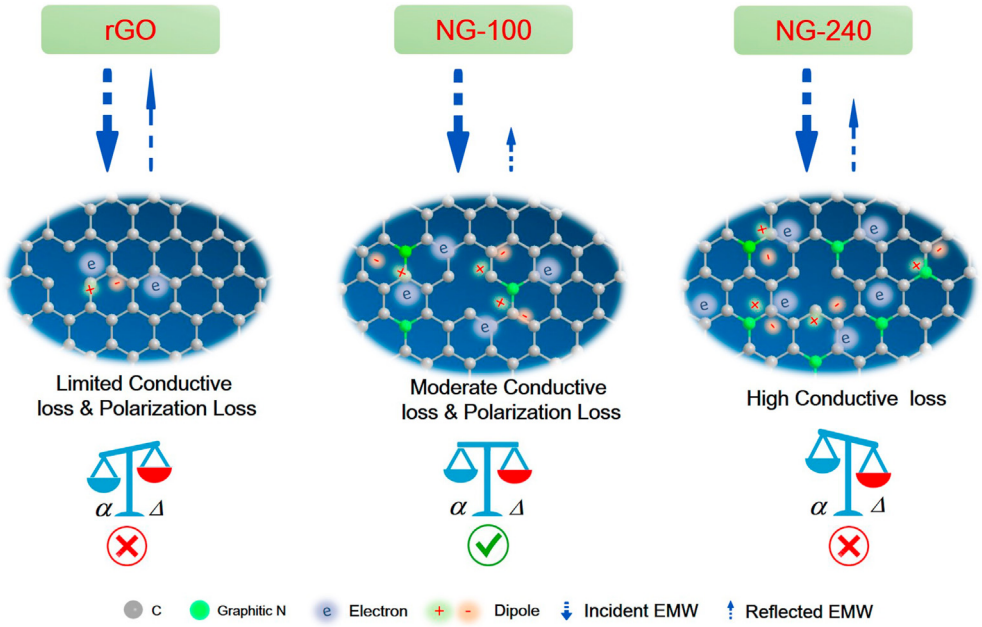

Fig. 9. Schematic illustration of EMW attenuation mechanisms in rGO and NG-X absorbers.

absorbers. In general, the microwave inside absorber (here the electric field stands for the microwave, and the intensity of electric field means the intendity of microwave inside) display the revise trend under the same fixed conditions and corroborate each other (*i.e.* the stronger magnetic field means the weaker electric field and vice versa) [52,53]. By comprehensive comparison, it is easy to observe that the moderate N-doped NG-100 exhibtes the optimal attenuation capacity compared to that of NG-240 and rGO. In addition, the gradual decreasing values of power loss density also confirms the gradual EMW consuming inside absorbers [52,54]. The above CST simulation results evidences the necessary of the balance between "α" and "Δ".

Generally, the attenuation ability of EMW absorbers is closely related to the degree of incident EMW absorptions and multiple internal reflection [13,27]. Based on the experimental and CST simulation results, Fig. 10 gives the schematic illustration of EMW attenuation mechanisms of rGO, NG-100 and NG-240 absorbers. Briefly, the "α" and "Δ" of graphene presents the N-doping content dependent properies. The non-doped graphene endows weak attenuation ability because of the limited conductive loss and dipole polariations. As a contrast, the moderate N-doped graphene (NG-100) was given the moderate conductive loss and N-doping caused dipole polarizations, thus presenting the better balance between "α" and "Δ". With the further increasing of N-doping content, however, the dramatical enhanced conductivity of heavy N-doped NG-240 lead to the deterioration of "Δ". As a result, the NG-240 also display the unmatched balance between "α" and "Δ". In addition, considering the similar 2D mophologies of three absorber, the scattering effect in those absorbers should also be give a positive effect in boosting the EMW attenuation [17,18]. Compared to the reported typical N-doped carbon-based absorbers as shown in Table S3, the NG-X absorbers presented in this work have the advantages of less loading and broadened EAB values. Considering the thin thickness, light weight, and enhanced EMW attenuation ability, the NG-X shows promising prospect in the area of microwave absorption.

4. Conclusions

In summary, the graphene with gradient N doping contents (0 wt%, 3.7 wt% and 6.86 wt%) have been prepared *via* hydrothermal reaction of GO with urea. The "α" and "Δ" of graphene presents the N-doping content dependent properies. Compared to the non-doped graphene, the moderate N-doped NG-100 presents the optimized EMW absorbing performance. The electromagnetic parameters and CST simulation results reveal that the boosted attenuation ability and well-optimized impedance characteristics should account for the enhanced EMW absorbing performance of NG-100. The RL_{max} of NG-100 with 5 wt% loading is up to ~ -55 dB and the EAB is as wide as ~6.82 GHz under 2.6 mm. The results evidence that the moderate N-doped content of graphene is of quite significance for adjusting the dielectric properties, attenuation factor and impedance matching properties of EMW absorbers, thus giving a combined and positive impact on EMW absorbing performance. The less loading, thinner thickness and broadened EAB of NG absorber demonstrate that the as-prepared NG are suitable candidates for high performance EMW absorbers.

CRediT authorship contribution statement

Mingqiang Ning: prepared and characterized the samples. **Boya Kuang:** Formal analysis, assisted with CST simulations and analysis of the results. **Lin Wang:** Formal analysis, assisted with CST simulations and analysis of the results. In addition, Mingqiang Ning and Boya Kuang co-wrote the manuscript. **Jingbo Li:** Supervision, designed and supervised this work. **Haibo Jin:** Supervision, designed and supervised this work.

Declaration of competing interest

The authors declare that they have no known competing financial interests or personal relationships that could have appeared to influence the work reported in this paper.

Acknowledgements

The authors gratefully acknowledge the financial support from National Natural Science Foundation of China (Grant NO.: 51972029; 51772029).

Appendix A. Supplementary data

Supplementary data related to this article can be found at https://doi.org/10.1016/j.jallcom.2020.157113.

References

[1] L.P. Renchao Che, Xiaofeng Duan, Qing Chen, Xuelei Liang, Microwave absorption enhancement and complex permittivity and permeability of Fe encapsulated within carbon nanotubes, Adv. Mater. 16 (2004) 401–404.
[2] W.L. Song, X.T. Guan, L.Z. Fan, W.Q. Cao, Q.L. Zhao, C.Y. Wang, M.S. Cao, Tuning broadband microwave absorption *via* highly conductive Fe_3O_4/graphene heterostructural nanofillers, Mater. Res. Bull. 72 (2015) 316–323.
[3] B. Wen, M.S. Cao, M.M. Lu, W.Q. Cao, H.L. Shi, J. Liu, X.X. Wang, H.B. Jin, X.Y. Fang, W.Z. Wang, J. Yuan, Reduced graphene oxides: light-weight and high-efficiency electromagnetic interference shielding at elevated temperatures, Adv. Mater. 26 (2014) 3484–3489.
[4] H. Chen, Z. Huang, Y. Huang, Y. Zhang, Z. Ge, B. Qin, Z. Liu, Q. Shi, P. Xiao, Y. Yang, T. Zhang, Y. Chen, Synergistically assembled MWCNT/graphene foam with highly efficient microwave absorption in both C and X bands, Carbon 124 (2017) 506–514.
[5] Y. Zhang, Y. Huang, T. Zhang, H. Chang, P. Xiao, H. Chen, Z. Huang, Y. Chen, Broadband and tunable high-performance microwave absorption of an ultralight and highly compressible graphene foam, Adv. Mater. 27 (2015) 2049–2053.
[6] Q. Liu, Q. Cao, H. Bi, C. Liang, K. Yuan, W. She, Y. Yang, R. Che, CoNi@SiO_2@TiO_2 and CoNi@air@TiO_2 microspheres with strong wideband microwave absorption, Adv. Mater. 28 (2016) 486–490.
[7] W.L. Song, M.S. Cao, M.M. Lu, J. Liu, J. Yuan, L.Z. Fan, Improved dielectric properties and highly efficient and broadened bandwidth electromagnetic attenuation of thickness-decreased carbon nanosheet/wax composites, J. Mater. Chem. C 1 (2013) 1846–1854.
[8] M. Ning, J. Li, B. Kuang, C. Wang, D. Su, Y. Zhao, H. Jin, M. Cao, One-step fabrication of N-doped CNTs encapsulating M nanoparticles (M = Fe, Co, Ni) for efficient microwave absorption, Appl. Surf. Sci. 447 (2018) 244–253.
[9] S.K. Singh, M.J. Akhtar, K.K. Kar, Hierarchical carbon nanotube-coated carbon fiber: ultra lightweight, thin, and highly efficient microwave absorber, ACS Appl. Mater. Interfaces 10 (2018) 24816–24828.
[10] W.Z. Nujiang Tang, Chaktong Au, Yi Yang, Mangui Han, Kuanjiuh Lin, Youwei Du, synthesis, microwave electromagnetic, and microwave absorption properties of twin carbon nanocoils, J. Phys. Chem. C 112 (2008) 19316–19323.
[11] J.P.F. Santos, M. Arjmand, G.H.F. Melo, K. Chizari, R.E.S. Bretas, U. Sundararaj, Electrical conductivity of electrospun nanofiber mats of polyamide 6/polyaniline coated with nitrogen-doped carbon nanotubes, Mater. Des. 141 (2018) 333–341.
[12] F. Sharif, M. Arjmand, A.A. Moud, U. Sundararaj, E.P.L. Roberts, Segregated hybrid poly(methyl methacrylate)/graphene/magnetite nanocomposites for electromagnetic interference shielding, ACS Appl. Mater. Interfaces 9 (2017) 14171–14179.
[13] J.Z. He, X.X. Wang, Y.L. Zhang, M.S. Cao, Small magnetic nanoparticles decorating reduced graphene oxides to tune the electromagnetic attenuation capacity, J. Mater. Chem. C 4 (2016) 7130–7140.
[14] X. Jian, B. Wu, Y. Wei, S.X. Dou, X. Wang, W. He, N. Mahmood, Facile synthesis of Fe_3O_4/GCs composites and their enhanced microwave absorption properties, ACS Appl. Mater. Interfaces 8 (2016) 6101–6109.
[15] J. Ma, X. Wang, W. Cao, C. Han, H. Yang, J. Yuan, M. Cao, A facile fabrication and highly tunable microwave absorption of 3D flower-like Co_3O_4-rGO hybrid-architectures, Chem. Eng. J. 339 (2018) 487–498.
[16] G. Chai, D. Xue, X. Fan, X. Li, D. Guo, Extending the Snoek's limit of single layer film in $(Co_{96}Zr_4/Cu)_n$ multilayers, Appl. Phys. Lett. 93 (152516) (2008) 152511–152513.
[17] P. Liu, Y. Zhang, J. Yan, Y. Huang, L. Xia, Z. Guang, Synthesis of lightweight N-doped graphene foams with open reticular structure for high-efficiency electromagnetic wave absorption, Chem. Eng. J. 368 (2019) 285–298.
[18] Z. Li, X. Li, Y. Zong, G. Tan, Y. Sun, Y. Lan, M. He, Z. Ren, X. Zheng, Solvothermal synthesis of nitrogen-doped graphene decorated by superparamagnetic Fe_3O_4 nanoparticles and their applications as enhanced synergistic microwave absorbers, Carbon 115 (2017) 493–502.
[19] Y. Qing, H. Nan, F. Luo, W. Zhou, Nitrogen-doped graphene and titanium carbide nanosheet synergistically reinforced epoxy composites as high-performance microwave absorbers, RSC Adv. 7 (2017) 27755–27761.
[20] M.M. Lu, M.S. Cao, Y.H. Chen, W.Q. Cao, J. Liu, H.L. Shi, D.Q. Zhang, W.Z. Wang, J. Yuan, Multiscale Assembly of grape-like ferroferric oxide and carbon nanotubes: a smart absorber prototype varying temperature to tune intensities, ACS Appl. Mater. Interfaces 7 (2015) 19408–19415.
[21] M. Arjmand, U. Sundararaj, Effects of nitrogen doping on X-band dielectric properties of carbon nanotube/polymer nanocomposites, ACS Appl. Mater. Interfaces 7 (2015) 17844–17850.
[22] Y. Duan, Z. Liu, H. Jing, Y. Zhang, S. Li, Novel microwave dielectric response of Ni/Co-doped manganese dioxides and their microwave absorbing properties, J. Mater. Chem. 22 (2012) 18291.
[23] J. Zhou, Y. Chen, H. Li, R. Dugnani, Q. Du, H. UrRehman, H. Kang, H. Liu, Facile synthesis of three-dimensional lightweight nitrogen-doped graphene aerogel with excellent electromagnetic wave absorption properties, J. Mater. Sci. 53 (2017) 4067–4077.
[24] S.A. Hasan, E.K. Tsekoura, V. Sternhagen, M. Strømme, Evolution of the composition and suspension performance of nitrogen-doped graphene, J. Phys. Chem. C 116 (2012) 6530–6536.
[25] M.P. Kumar, T. Kesavan, G. Kalita, P. Ragupathy, T.N. Narayanan, D.K. Pattanayak, On the large capacitance of nitrogen doped graphene derived by a facile route, RSC Adv. 4 (2014) 38689–38697.
[26] P. Chamoli, S.K. Singh, M.J. Akhtar, M.K. Das, K.K. Kar, Nitrogen doped graphene nanosheet-epoxy nanocomposite for excellent microwave absorption, Phys. E Low-dimens. Syst. Nanostruct. 103 (2018) 25–34.
[27] X. Zhang, J. Xu, H. Yuan, S. Zhang, Q. Ouyang, C. Zhu, X. Zhang, Y. Chen, Large-scale synthesis of three-dimensional reduced graphene oxide/nitrogen-doped carbon nanotube heteronanostructures as highly efficient electromagnetic wave absorbing materials, ACS Appl. Mater. Interfaces 11 (2019) 39100–39108.
[28] X. Zhang, X. Zhang, D. Wang, H. Yuan, S. Zhang, C. Zhu, X. Zhang, Y. Chen, Three dimensional graphene-supported nitrogen-doped carbon nanotube architectures for attenuation of electromagnetic energy, J. Mater. Chem. C 7 (2019) 11868–11878.
[29] S.K. Singh, H. Prakash, M.J. Akhtar, K.K. Kar, Lightweight and high-performance microwave absorbing heteroatom-doped carbon derived from chicken feather fibers, ACS Sustain. Chem. Eng. 6 (2018) 5381–5393.
[30] N. Yang, Z.X. Luo, G.R. Zhu, S.C. Chen, X.L. Wang, G. Wu, Y.Z. Wang, Ultralight three-dimensional hierarchical cobalt nanocrystals/N-doped CNTs/carbon sponge composites with a hollow skeleton toward superior microwave absorption, ACS Appl. Mater. Interfaces 11 (2019) 35987–35998.
[31] S. Pei, H.-M. Cheng, The reduction of graphene oxide, Carbon 50 (2012) 3210–3228.
[32] L. Sun, L. Wang, C. Tian, T. Tan, Y. Xie, K. Shi, M. Li, H. Fu, Nitrogen-doped graphene with high nitrogen level via a one-step hydrothermal reaction of graphene oxide with urea for superior capacitive energy storage, RSC Adv. 2 (2012) 4498.
[33] J.Y. Guoxiu Wang, Jinsoo Park, Xinglong Gou, Bei Wang, Hao Liu, Jane Yao, Facile synthesis and characterization of graphene nanosheets, J. Phys. Chem. C 112 (2008) 8192–8195.
[34] N.A. Kumar, H. Nolan, N. McEvoy, E. Rezvani, R.L. Doyle, M.E.G. Lyons, G.S. Duesberg, Plasma-assisted simultaneous reduction and nitrogen doping of graphene oxide nanosheets, J. Mater. Chem. 1 (2013) 4431.
[35] J.C. Meyer, A.K. Geim, M.I. Katsnelson, K.S. Novoselov, T.J. Booth, S. Roth, The structure of suspended graphene sheets, Nature 446 (2007) 60–63.
[36] B. Kuang, W. Song, M. Ning, J. Li, Z. Zhao, D. Guo, M. Cao, H. Jin, Chemical reduction dependent dielectric properties and dielectric loss mechanism of reduced graphene oxide, Carbon 127 (2018) 209–217.
[37] D. Yang, A. Velamakanni, G. Bozoklu, S. Park, M. Stoller, R.D. Piner, S. Stankovich, I. Jung, D.A. Field, C.A. Ventrice, R.S. Ruoff, Chemical analysis of graphene oxide films after heat and chemical treatments by X-ray photoelectron and Micro-Raman spectroscopy, Carbon 47 (2009) 145–152.
[38] Z.X. Li Li Zhang, X.S. Zhao, Pillaring chemically exfoliated graphene oxide with carbon nanotubes for photocatalytic degradation of dyes under visible light irradiation, ACS Nano 4 (2010) 7030–7036.
[39] D. Kim, S.J. Yang, Y.S. Kim, H. Jung, C.R. Park, Simple and cost-effective reduction of graphite oxide by sulfuric acid, Carbon 50 (2012) 3229–3232.
[40] X. Xu, T. Yuan, Y. Zhou, Y. Li, J. Lu, X. Tian, D. Wang, J. Wang, Facile synthesis of boron and nitrogen-doped graphene as efficient electrocatalyst for the oxygen reduction reaction in alkaline media, Int. J. Hydrogen Energy 39 (2014) 16043–16052.
[41] K.S. Mali, J. Greenwood, J. Adisoejoso, R. Phillipson, S. De Feyter, Nanostructuring graphene for controlled and reproducible functionalization, Nanoscale 7 (2015) 1566–1585.
[42] M. Pykal, P. Jurecka, F. Karlicky, M. Otyepka, Modelling of graphene functionalization, Phys. Chem. Chem. Phys. : Phys. Chem. Chem. Phys. 18 (2016) 6351–6372.
[43] J. Feng, F. Pu, Z. Li, X. Li, X. Hu, J. Bai, Interfacial interactions and synergistic effect of CoNi nanocrystals and nitrogen-doped graphene in a composite microwave absorber, Carbon 104 (2016) 214–225.
[44] H. Yuan, B. Li, C. Zhu, Y. Xie, Y. Jiang, Y. Chen, Dielectric behavior of single iron atoms dispersed on nitrogen-doped nanocarbon, Appl. Phys. Lett. 116 (153101) (2020) 153101, 153101(153104).
[45] J. Yan, Y. Huang, C. Chen, X. Liu, H. Liu, The 3D CoNi alloy particles embedded in N-doped porous carbon foams for high-performance microwave absorbers, Carbon 152 (2019) 545–555.
[46] J. Yan, Y. Huang, Y. Yan, L. Ding, P. Liu, High-performance electromagnetic wave absorbers based on two kinds of nickel-based MOF-derived Ni@C microspheres, ACS Appl. Mater. Interfaces 11 (2019) 40781–40792.
[47] H. Yuan, X. Zhang, F. Yan, S. Zhang, C. Zhu, C. Li, X. Zhang, Y. Chen, Nitrogen-

doped carbon nanosheets containing Fe_3C nanoparticles encapsulated in nitrogen-doped graphene shells for high-performance electromagnetic wave absorbing materials, Carbon 140 (2018) 368–376.
[48] X. Hong, Q. Wang, Z. Tang, W.Q. Khan, D. Zhou, T. Feng, Synthesis and electromagnetic absorbing properties of titanium carbonitride with quantificational carbon doping, J. Phys. Chem. C 120 (2015) 148–156.
[49] H. Xing, Z. Liu, L. Lin, L. Wang, D. Tan, Y. Gan, X. Ji, G. Xu, Excellent microwave absorption properties of Fe ion-doped SnO_2/multi-walled carbon nanotube composites, RSC Adv. 6 (2016) 41656–41664.
[50] L. Cui, C. Tian, L. Tang, X. Han, Y. Wang, D. Liu, P. Xu, C. Li, Y. Du, Space-confined synthesis of core-shell $BaTiO_3$@Carbon microspheres as a high-performance binary dielectric system for microwave absorption, ACS Appl. Mater. Interfaces 11 (2019) 31182–31190.
[51] Z. Ma, C.T. Cao, Q.F. Liu, J.B. Wang, A new method to calculate the degree of electromagnetic impedance matching in one-layer microwave absorbers, Chin. Phys. Lett. 29 (2012), 038401, 038401-038404.
[52] F. Ye, C. Song, Q. Zhou, X. Yin, M. Han, X. Li, L. Zhang, L. Cheng, Broadband microwave absorbing composites with a multi-scale layered structure based on reduced graphene oxide film as the frequency selective surface, Materials 11 (2018) 1–12.
[53] A. Ling, G. Tan, Q. Man, Y. Lou, S. Chen, X. Gu, R.-W. Li, J. Pan, X. Liu, Broadband microwave absorbing materials based on MWCNTs' electromagnetic wave filtering effect, Compos. B Eng. 171 (2019) 214–221.
[54] K.-L. Zhang, J.-Y. Zhang, Z.-L. Hou, S. Bi, Q.-L. Zhao, Multifunctional broadband microwave absorption of flexible graphene composites, Carbon 141 (2019) 608–617.